

# UC Berkeley

## UC Berkeley Previously Published Works

### Title

Electron-hole Hybridization in Bilayer Graphene

### Permalink

<https://escholarship.org/uc/item/10x6w1m5>

### Journal

National Science Review, 7(2)

### ISSN

2095-5138

### Authors

Wang, Siqi

Zhao, Mervin

Zhang, Changjian

et al.

### Publication Date

2020-02-01

### DOI

10.1093/nsr/nwz212

### Copyright Information

This work is made available under the terms of a Creative Commons Attribution License, available at <https://creativecommons.org/licenses/by/4.0/>

Peer reviewed

## PHYSICS

# Electron-hole hybridization in bilayer graphene

Siqi Wang<sup>1,2</sup>, Mervin Zhao<sup>1,2</sup>, Changjian Zhang<sup>3</sup>, Sui Yang<sup>1,2</sup>, Yuan Wang<sup>1,2</sup>, Kenji Watanabe<sup>4</sup>, Takashi Taniguchi<sup>4</sup>, James Hone<sup>3</sup> and Xiang Zhang<sup>1,2,5,\*</sup>

## ABSTRACT

Band structure determines the motion of electrons in a solid, giving rise to exotic phenomena when properly engineered. Drawing an analogy between electrons and photons, artificially designed optical lattices indicate the possibility of a similar band modulation effect in graphene systems. Yet due to the fermionic nature of electrons, modulated electronic systems promise far richer categories of behaviors than those found in optical lattices. Here, we uncovered a strong modulation of electronic states in bilayer graphene subject to periodic potentials. We observed for the first time the hybridization of electron and hole sub-bands, resulting in local band gaps at both primary and secondary charge neutrality points. Such hybridization leads to the formation of flat bands, enabling the study of correlated effects in graphene systems. This work may provide a novel way to manipulate electronic states in layered systems, which is important to both fundamental research and application.

**Keywords:** band modulation, periodic potential, bilayer graphene

## INTRODUCTION

The behavior of ballistic electrons in a uniform material resembles that of photons to a high degree [1–7]. For example, electrons follow straight trajectories when considered as particles [8–11], while interference effects, such as the Aharonov–Bohm [11–13] and Fabry–Perot effects [14], are caused by their wave nature. Due to the conservation of the transverse momentum and the Fermi energy, electron propagation at the boundary of two regions with different carrier densities is subject to reflection and refraction in a way similar to optical rays crossing the boundary of two materials with different refractive indices [15]. Unlike photons, electrons in an atomically thin material can be efficiently manipulated by an artificially designed and applied potential profile that controls the spatial carrier density profile [16–18], resulting in graphene electron optics. This opened the way to realizing scenarios that are typically difficult to achieve by traditional optics, such as negative refractive index and non-linear dispersion, in solid-state systems like graphene [19,20].

So far, research in graphene electron optics has focused on the single-interface effects, including the Veselago lens [15,19,20] and whispering gallery

[21]. However, modern optics has utilized the concept of superlattices (SLs) in photonic crystals, to achieve new optical phenomena. For example, the modulation of photonic states in one dimension by periodicity dramatically alters the photonic dispersion relation, which leads to commonly used dielectric mirrors, or the distributed Bragg reflector [22]. Moreover, in-plane photonic SLs have been utilized to demonstrate novel physics, such as topological electromagnetic states [23]. However, there are few experimental studies of SL effects in electronic systems, mostly in periodic quantum well structures [24]. Yet it limits the electrostatic modulation only along its growth axis. In this work, by employing a bipolar SL modulation in high-quality BLG, which exhibits a touching-hyperbolic dispersion that can be effectively modified electrostatically, we discovered a strong band modulation effect. For the first time, we demonstrate hybridization of electron and hole sub-bands causing emergence of local band gaps of several milli-electron volts around both the primary and secondary charge neutrality points. Such a hybridization leads to the formation of flat bands around local gaps, providing a platform for the study of strongly correlated effects in graphene systems [1–3].

<sup>1</sup>NSF Nanoscale Science and Engineering Center (NSEC), University of California, Berkeley, CA 94720, USA;

<sup>2</sup>Materials Sciences Division, Lawrence Berkeley National Laboratory, Berkeley, CA 94720, USA;

<sup>3</sup>Department of Mechanical Engineering, Columbia University, New York, NY 10027, USA;

<sup>4</sup>National Institute for Materials Science, Tsukuba, Japan and

<sup>5</sup>Faculties of Sciences and Engineering, University of Hong Kong, Hong Kong, China

\*Corresponding author. E-mail: [xzhang@me.berkeley.edu](mailto:xzhang@me.berkeley.edu)

Received 30 October 2019; Revised 5 December 2019;

Accepted 5 December 2019

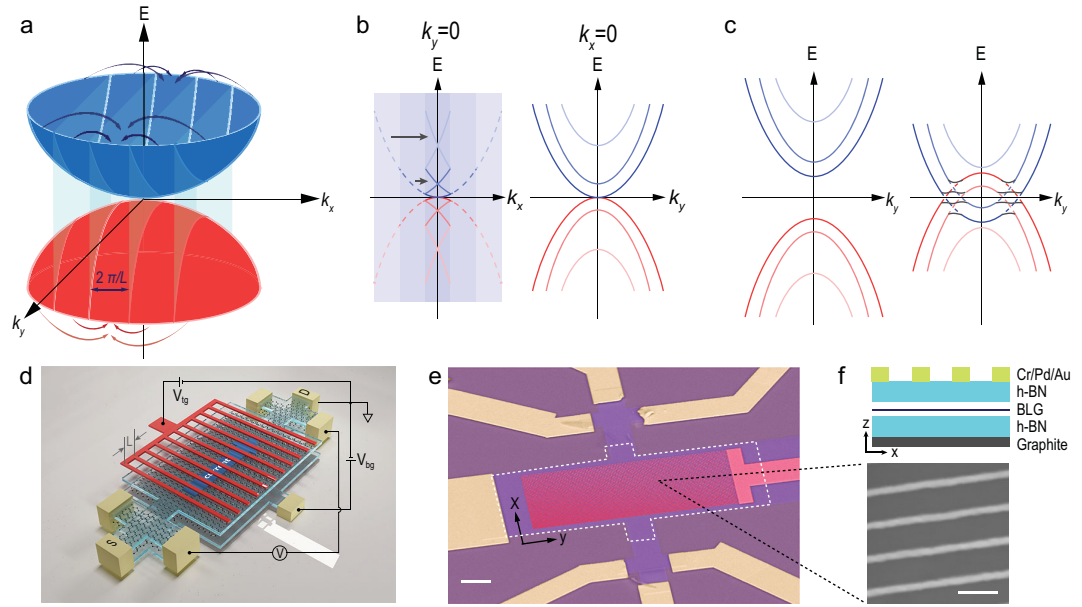


**Figure 1.** Band modification and artificial 1D superlattice in a BLG field-effect transistor with dual gates. (a) Schematic of band folding of BLG dispersion with an artificial periodicity  $L$  along the  $x$  direction, where the length of the reduced Brillouin zone along  $x$  becomes  $2\pi/L$ . (b) While bands along  $k_x$  are folded into the reduced Brillouin zone, electron and hole sub-bands extend along  $k_y$ . (c) Two different modulation regimes. In the monopolar regime, the same type of carrier was doped into the system and the bands were shifted, as in the case of homogeneous dual gate doping (left). In the bipolar doping regime, electron and hole states appeared at the Fermi surface simultaneously and sub-bands overlapped. Local band gaps appeared at the intersections. (d) Schematic perspective view of the device. (e) SEM image of a dual-gate FET device (scale bar:  $2\ \mu\text{m}$ ). BLG (blue) and the graphite bottom gate (marked by white dashed line) were connected via metal electrodes (yellow) via edge contacts. The metallic periodic top gate (red) covered the channel region. The scale bar is  $2\ \mu\text{m}$ . (f) Schematic cross-sectional view of the device and SEM image of the periodic top gate (scale bar:  $100\ \text{nm}$ ). The period of the SL was  $120\ \text{nm}$  with a metal width of  $25\ \text{nm}$ . The top h-BN had a thickness of  $25\ \text{nm}$  and the bottom one had a thickness of  $11\ \text{nm}$ .

Similar to a photonic crystal [25,26], artificial periodicity in a 2D material system induces band folding in the underlying dispersion of the pristine lattice [1,27]. In the case of BLG, the original hyperbolic dispersion is folded into the reduced Brillouin zone, forming sub-bands as shown in Fig. 1a and b. Moreover, in an electronic system, changes in the potential profile shift the electron sub-bands and hole sub-bands relative to the Fermi level, causing charge doping [28]. Depending on the sign of the potential profile, in general, there are two modulation regimes, namely monopolar modulation (Fig. 1c left), where carriers of the same type are doped into the system, and bipolar modulation (Fig. 1c right), where both types of carriers are doped in different spatial regions. While the monopolar modulation shifts electron and hole sub-bands similar to the gating effect of a uniformly gated BLG, we show that bipolar modulation causes intersection of electron and hole sub-bands due to the simultaneous appearance of electron and hole states around the Fermi surface. In this scenario, the dispersion of BLG is significantly modified. As a consequence, confirmed by our charge transport measurements and calculations,

local band gaps open at the crossing of electron and hole sub-bands resulting in sub-band hybridization in BLG.

## RESULTS

The encapsulation of 2D materials between hexagonal boron nitride (h-BN) can greatly improve device performance and protect the material from unwanted contamination [29]. Similarly, we encapsulated BLG between h-BN flakes using the van der Waals dry transfer technique and the periodic SL was created electrostatically (Fig. 1d–f). BLG was chosen because the presence of Klein tunneling in monolayer graphene results in the absence of local gap openings. The featureless back gate homogeneously doped the channel, whereas the periodic top gate independently induced density modulation in the BLG. All our devices are made with more than 60 metal lines to ensure good periodicity. In order to align the Fermi level at different positions with the ground, the electrons in BLG were subjected to an electrostatic potential  $U(x)$ , which fulfills  $-eU(x) + E(k_F(x)) = 0$ . The precise potential profile depends on the thickness of h-BN

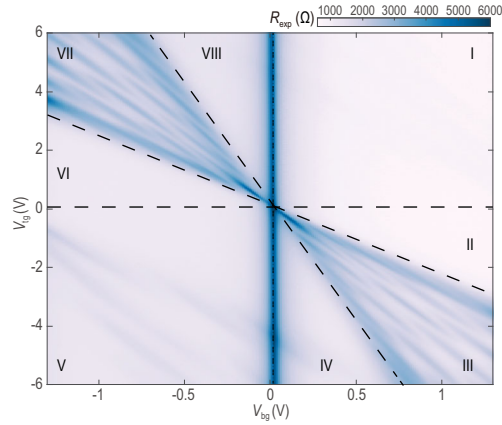


**Figure 2.** Transport behavior in a BLG SL. Color plot of the longitudinal resistance as a function of  $V_{tg}$  and  $V_{bg}$ . The black dashed lines separate different doping regimes of top and bottom gates.

flakes, the top-gate voltage  $V_{tg}$ , and the back-gate voltage  $V_{bg}$ .

The electronic modulation can be directly measured by electron transport in the device using a four-terminal lock-in technique at a temperature of 1.8 K. Transport measurements from a device with a SL period of 120 nm are shown in Fig. 2, where the measured resistance is plotted as a function of  $V_{tg}$  and  $V_{bg}$ . Applying a  $V_{tg}$  ‘turns on’ the SL potential, and two patterns can be observed (more data are shown in Fig. S1 in the online supplementary material). The first feature to note is the appearance of a bright vertical line at  $V_{bg} = 0$ , corresponding to the primary charge neutral point (CNP). Since the graphitic back gate extends across both the channel and contact areas, whereas the top-gate covers only the channel region (Fig. 1d), the position of the bright vertical line is independent of top-gate tuning.

More interestingly, two groups of clear patterns were observed to fan out diagonally from the CNP. This is very different from transport results obtained using a conventional BLG device with a featureless top gate and back gate, where we would expect only one diagonal line corresponding to the tuning of central CNP. In our device with a patterned top gate, we identified eight regions (I–VIII in Fig. 2) around the main CNP and interpreted them as eight doping regimes induced by the two gates. In the typical monopolar modulation regime, region I (V), two gates electrostatically doped electrons (holes) into BLG resulting in low resistance. A similar situation occurred at weak SL potentials (region II or VI), where the resistance was not significantly changed by the top gate because it did not affect carriers of the opposite type. As we increased the SL such that  $V_{tg}$  and  $V_{bg}$  were comparable in strength (region III or VII), the bipolar doping regime, associated with

regions II–IV (VI–VIII), was achieved. The contact and channels became electron (hole) doped from the back gate, whereas the top gate selectively doped holes (electrons) electrostatically. Electron and hole states appeared at the Fermi level along the SL direction. Therefore, the effective potential  $U(x)$  oscillated between positive and negative values as a function of the position  $x$ . These two regions were found where the strongest SL modulation was expected, resulting in the clear woven pattern in the fan area.

We attribute the observed phenomenon to the dispersion modulation due to the simultaneous appearance of electron and hole states around the Fermi surface. The original hyperbolic BLG band structure has been greatly modified by the SL potential (Fig. 1c). Spatial changes in the effective potential created an overlap between original electron-like and hole-like bands and caused them to intersect. Local gaps opened in the electronic spectrum around  $k_y = 0$ , with no states in the gap region at any value of  $k_x$ . Even though allowed electronic states still exist at large  $|k_y|$ , they do not contribute to transport in the device, since the bandwidth along  $k_x$  rapidly shrinks to zero. When the Fermi level lies inside (outside) the newly created local gap, which can be achieved by tuning  $V_{bg}$  and  $V_{tg}$ , the device has higher (lower) resistance.

In the experiment, at each negative  $V_{bg}$ , as the SL potential increased, the overlap between electron-like and hole-like bands increased gradually, which caused different local gaps to coincide with the Fermi level. It is this oscillatory nature of overlaps between the two bands that lies at the origin of the observed woven pattern. Due to the nature of band hybridization, we suggest states around local gaps appeared as a superposition, whereas states far away from local gaps were generally composed of either electron or hole. It is the introduction of the periodic potential that led to the intersection and hybridization of electron and hole sub-bands to form new electronic states in the reduced Brillouin zone. The hybridization resulted in the appearance of local band gaps and mixed states.

We also noticed the appearance of a weak resistance modulation in regions I and V. Interestingly, as we increased  $V_{bg}$ , the weak pattern could be identified as part of a similar woven pattern centered at  $V_{bg} = \pm 1.5$  V. In the full-range resistance map (Fig. 3a), we observed three sets of repeated patterns in total. We attributed the two new bright vertical lines to secondary CNPs of BLG, which were caused by the moiré pattern forming between BLG and h-BN. According to the above analysis, the SL effect was imposed into the system via carrier density modulation. Similar gap-opening effects may also occur elsewhere, as long as the carrier modulation remains

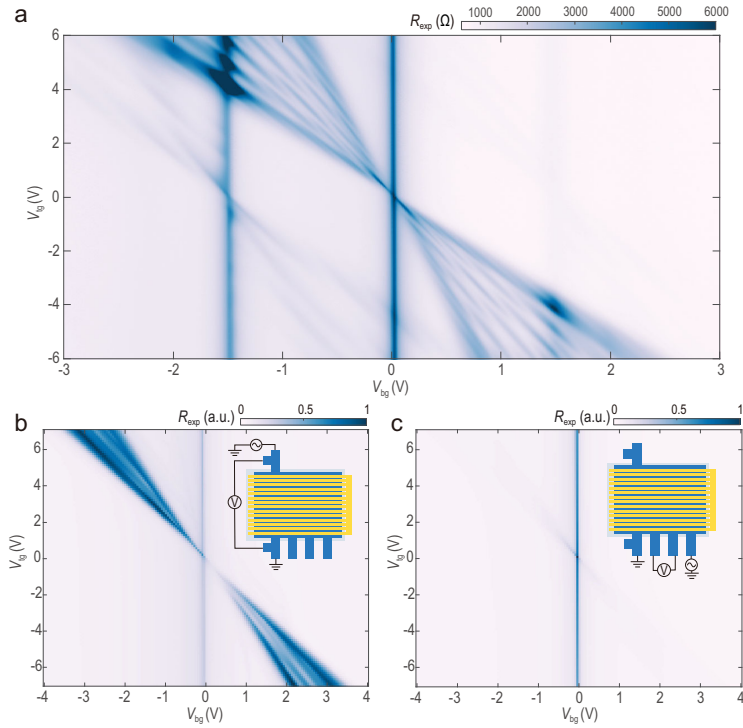


**Figure 3.** Full range resistance mapping and the direction dependence of SL modulation effect. (a) Full range resistance mapping showed three repeated sets of patterns originating from the main CNP at  $(V_{bg}, V_{tg}) = (0, 0)$ , and secondary CNPs at  $(\pm 1.5 \text{ V}, 0)$ . (b) Resistance mapping with the current parallel to the periodicity showed a similar modulation pattern as in (a). (c) Resistance mapping with the current perpendicular to the periodicity only showed very weak modulation possibly due to imperfect geometry of the device or stray current. Insets in (b) and (c) are device and measurement schematics.

bipolar. Around the secondary CNPs, electrons and holes can be doped into the system as easily as near the primary CNP, which we have indeed achieved in the experiment.

On the other hand, since the potential in BLG is modulated only along one direction, we do not expect any change in transport properties normal to that direction. To confirm this reasoning, we fabricated another device with a different geometry, which allows the measurement of transport both along the direction of modulation and normal to that direction. Our results are shown in Fig. 3b and c. Whereas the resistance along the direction of the modulation (Fig. 3b) showed a similar woven pattern as that displayed in Fig. 2a, the resistance map along a direction normal to that (Fig. 3c) indicated merely a shift of the CNP under the combined influence of the top and the back gate.

Formation of local gaps in the spectrum was further confirmed by temperature-dependent measurements. Changes in the channel resistance at  $V_{bg} = -0.55 \text{ V}$  as a function of  $V_{tg}$  are shown in Fig. 4 in the temperature range from 1.8 K to 51.8 K. The oscillation in the woven pattern becomes flatter at

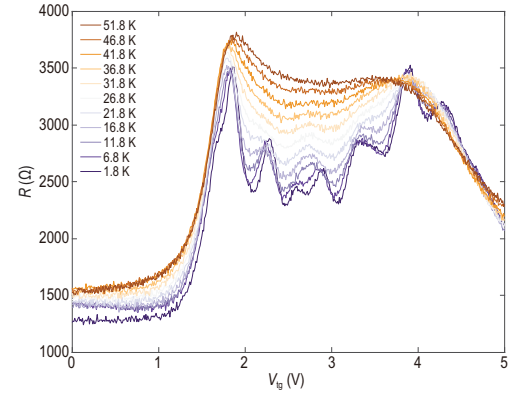


**Figure 4.** Temperature dependence of BLG SL FET. Perpendicular resistance of the device shown in Fig. 2 at  $V_{bg} = -0.55 \text{ V}$  with temperature ranging from 1.8 K to 51.8 K. The oscillation in the woven pattern became flatter at higher temperature and smeared out around 25 K, corresponding to an activation energy of 2 meV.

higher temperatures, indicating that the effect of the SL potential decreases at higher temperatures due to thermal fluctuations, causing excitation of electrons across local band gaps at elevated temperatures. At high temperatures, the woven pattern in the resistance map washes out and changes to a normal high-resistance behavior of BLG transistors with a featureless dual gate. The woven pattern is completely suppressed beyond about 25 K, corresponding to a gap or activation energy of 2 meV, in quantitative agreement with the theoretical results. We consider this finding to provide independent support for the adequacy of the theoretical description of this complex system that matches well with the experimental results.

## CONCLUSION

We have demonstrated strong modification of the BLG band structure by an artificial, electrostatically induced SL potential. Periodicity imposed by the SL led to band folding in the original band dispersion of BLG. In a regime of bipolar carrier density modulation, electron and hole states strongly hybridize and locally open band gaps around the Fermi level, which can persist up to 25 K. Owing to the large flexibility in the device design, the paradigm of modulating the electrostatic potential in the channel region may be generalized to higher dimensions and utilized to realize more exotic electronic phenomena.

## METHODS

The h-BN flakes were chosen with thickness ranging between 10 and 30 nm to ensure excellent gate insulation and modulation amplitude. The

h-BN/BLG/h-BN stack was then transferred on few-layer graphite, which served as the conductive back gate in the measurement. To create our electrostatically defined potential, we used electron beam lithography to define a SL with a period of 120 nm and linewidth of 25 nm. The period length was chosen by considering both the lithography precision and the integrity of the structure after the following lift-off process. Prior to the standard PMMA spin-coating process, the stack was treated with mild oxygen plasma and HMDS to enhance the adhesion between the top h-BN surface and PMMA. Transport measurements were performed using the Physical Property Measurement System from Quantum Design with a base temperature of 1.8 K. Our four-probe measurements employed both low-frequency lock-in techniques (13.3 Hz frequency and AC excitation current of 10–100 nA) and DC measurement, both of which gave consistent results.

## SUPPLEMENTARY DATA

Supplementary data are available at [NSR](#) online.

## FUNDING

S.W., M.Z., S.Y., Y.W. and X.Z. acknowledge the support from the U.S. Department of Energy, Office of Science, Office of Basic Energy Sciences, Materials Sciences and Engineering Division within the van der Waals Heterostructures Program (KCWF16) under contract No. DEAC02-05-CH11231 for sample preparation, the support from the National Science Foundation (NSF) MRI grant 1725335 for low-temperature measurement, and the support from the King Abdullah University of Science and Technology (KAUST) Office of Sponsored Research award OSR-2016-CRG5-2996 for sample fabrication. C.Z. and J.H. acknowledge the support from NSF EFMA-1741660. K.W. and T.T. acknowledge the support from the Elemental Strategy Initiative conducted by the Ministry of Education, Culture, Sports, Science and Technology (MEXT), Japan, and CREST (JP-MJCR15F3), Japan Science and Technology Agency (JST).

**Conflict of interest statement.** None declared.

## REFERENCES

- Bistritzer R and MacDonald AH. Moire bands in twisted double-layer graphene. *Proc Natl Acad Sci USA* 2011; **108**: 12233–7.
- Cao Y, Fatemi V and Demir A *et al.* Correlated insulator behaviour at half-filling in magic-angle graphene superlattices. *Nature* 2018; **556**: 80–4.
- Cao Y, Fatemi V and Fang S *et al.* Unconventional superconductivity in magic-angle graphene superlattices. *Nature* 2018; **556**: 43–50.
- Ribeiro-Palau R, Zhang C and Watanabe K *et al.* Twistable electronics with dynamically rotatable heterostructures. *Science* 2018; **361**: 690–3.
- Yankowitz M, Jung J and Laksono E *et al.* Dynamic band-structure tuning of graphene moiré superlattices with pressure. *Nature* 2018; **557**: 404–8.
- Yankowitz M, Ma Q and Jarillo-Herrero P *et al.* van der Waals heterostructures combining graphene and hexagonal boron nitride. *Nat Rev Phys* 2019; **1**: 112–25.
- Dragoman D and Dragoman M. Optical analogue structures to mesoscopic devices. *Prog Quantum Electron* 1999; **23**: 131–88.
- Banszerus L, Schmitz M and Engels S *et al.* Ballistic transport exceeding 28  $\mu\text{m}$  in CVD grown graphene. *Nano Lett* 2016; **16**: 1387–91.
- Baringhaus J, Ruan M and Edler F *et al.* Exceptional ballistic transport in epitaxial graphene nanoribbons. *Nature* 2014; **506**: 349–54.
- Lee M, Wallbank JR and Gallagher P *et al.* Ballistic miniband conduction in a graphene superlattice. *Science* 2016; **353**: 1526–9.
- Dauber J, Oellers M and Venn F *et al.* Aharonov-Bohm oscillations and magnetic focusing in ballistic graphene rings. *Phys Rev B* 2017; **96**: 205407.
- de Juan F, Cortijo A and Vozmediano MAH *et al.* Aharonov-Bohm interferences from local deformations in graphene. *Nat Phys* 2011; **7**: 810–5.
- Smirnov D, Schmidt H and Haug RJ. Aharonov-Bohm effect in an electron-hole graphene ring system. *Appl Phys Lett* 2012; **100**: 203114.
- Young AF and Kim P. Quantum interference and Klein tunnelling in graphene heterojunctions. *Nat Phys* 2009; **5**: 222–6.
- Cheianov VV, Fal'ko V and Altshuler BL. The focusing of electron flow and a veselago lens in graphene p-n junctions. *Science* 2007; **315**: 1252–5.
- Li J, Wang K and McFaul KJ *et al.* Gate-controlled topological conducting channels in bilayer graphene. *Nat Nanotech* 2016; **11**: 1060–5.
- Li J, Wen H and Watanabe K *et al.* Gate-controlled transmission of quantum hall edge states in bilayer graphene. *Phys Rev Lett* 2018; **120**: 57701.
- Forsythe C, Zhou X and Watanabe K *et al.* Band structure engineering of 2D materials using patterned dielectric superlattices. *Nat Nanotechnol* 2018; **13**: 566–71.
- Chen S, Han Z and Elahi MM *et al.* Electron optics with p-n junctions in ballistic graphene. *Science* 2016; **353**: 1522–5.
- Lee G-H, Park G-H and Lee H-J. Observation of negative refraction of Dirac fermions in graphene. *Nat Phys* 2015; **11**: 925–9.
- Zhao Y, Wyrick J and Natterer FD *et al.* Creating and probing electron whispering-gallery modes in graphene. *Science* 2015; **348**: 672–5.
- Sheppard CJR. Approximate calculation of the reflection coefficient from a stratified medium. *Pure Appl Opt* 1995; **4**: 665–9.
- Wang Z, Chong Y and Joannopoulos JD *et al.* Observation of unidirectional backscattering-immune topological electromagnetic states. *Nature* 2009; **461**: 772–5.

24. Fox M and Ispasoiu R. Quantum wells, superlattices, and band-gap engineering. In: Kasap S and Capper P (eds). *Springer Handbook of Electronic and Photonic Materials*. 2nd edn. Cham: Springer, 2017, 1037–55.
25. Yablonovitch E. Inhibited spontaneous emission in solid-state physics and electronics. *Phys Rev Lett* 1987; **58**: 2059–62.
26. John S. Strong localization of photons in certain disordered dielectric superlattices. *Phys Rev Lett* 1987; **58**: 2486–9.
27. Moon P and Koshino M. Electronic properties of graphene/hexagonal-boron-nitride moiré superlattice. *Phys Rev B* 2014; **90**: 155406.
28. Novoselov KS, Geim AK and Morozov SV *et al.* Two-dimensional gas of massless Dirac fermions in graphene. *Nature* 2005; **438**: 197–200.
29. Wang L, Meric I and Huang PY *et al.* One-dimensional electrical contact to a two-dimensional material. *Science* 2013; **342**: 614–7.